

# Discrete Diffusion Models Exploit Asymmetry to Solve Lookahead Planning Tasks

Itamar Trainin<sup>1</sup> Shauli Ravfogel<sup>2</sup> Omri Abend<sup>1</sup> Amir Feder<sup>1</sup>

## Abstract

While Autoregressive (AR) Transformer-based Generative Language Models are frequently employed for lookahead tasks, recent research suggests a potential discrepancy in their ability to perform planning tasks that require multi-step lookahead. In this work, we investigate the distinct emergent mechanisms that arise when training AR versus Non-Autoregressive (NAR) models, such as Discrete Diffusion Models (dLLMs), on lookahead tasks. By requiring the models to plan ahead to reach the correct conclusion, we analyze how these two paradigms fundamentally differ in their approach to the problem. We identify a critical asymmetry in planning problems: while forward generation requires complex lookahead at branching junctions, reverse generation is often deterministic. This asymmetry creates an opportunity for NAR models. Through mechanistic analysis of training and inference dynamics, we demonstrate that NAR models learn to solve planning tasks by utilizing future tokens to decode backwards, avoiding the need to learn complex traversal mechanisms entirely. Consequently, we report that both AR and NAR models are able to achieve perfect accuracy on the lookahead task. However, NAR models require exponentially fewer training examples and shallower architectures compared to AR models, which often fail to converge without specific curriculum adjustments.

## 1. Introduction

The ability to plan a valid path towards reaching a desired goal is a fundamental requirement for complex decision-based systems (Valmeekam et al., 2023). To successfully plan, an agent must maintain a model of potential state transitions, understanding not just immediate effects but

<sup>1</sup>Hebrew University of Jerusalem <sup>2</sup>New York University. Correspondence to: Itamar Trainin <itamar.trainin@mail.huji.ac.il>.

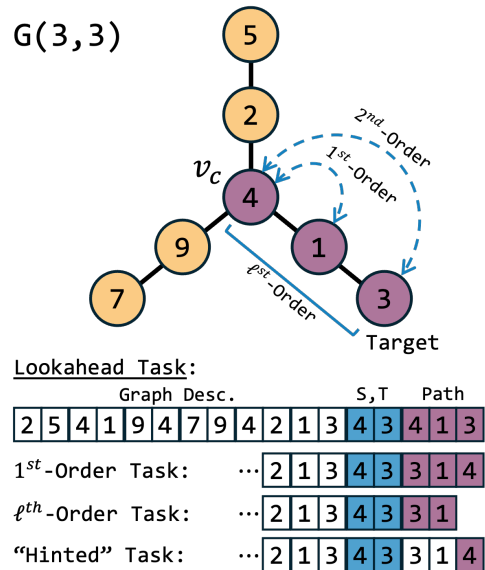


Figure 1. Depiction of a lookahead Star-Graph with 3 arms and 3 vertices in each arm, and a visualization of its tokenized sequence format for *Original* lookahead task, 1<sup>st</sup> - Order task where the path is decoded in reverse,  $\ell^{\text{th}}$  - Order task where only the first and second vertices are predicted and "Hinted" task where the true first and second vertices are provided in context. Purple indicates tokens predicted at test time.

how current choices constrain future possibilities (Gao et al., 2024; Erdogan et al., 2025). Although Autoregressive (AR) modeling is the current standard for Large Language Models (LLMs), a recent line of work suggests that the causal "next-token" training objective poses an inherent conflict with the requirements of planning (Bachmann et al., 2024; Nie et al., 2025; Ye et al., 2025; 2024a).

One such instance is the Star-Path task (Bachmann et al., 2024). This task allows the study of how LLMs plan by creating an analogy of the model's complex decision-making process to simple graph algorithms. By drawing a connection between an LLM's internal world model and an associative memory, the decision process is modeled as a graph traversal task where the plan is the path connecting the source and target vertices. By introducing junctions to the graph, the correct path can only be determined by

fully exploring all rollouts. Thus, by designing the data as sequences that include (1) a textual graph description, (2) a definition of the source and target vertices, and (3) a description of the path connecting the source to the target, we reduce the planning problem to a graph-traversal problem. This framework enables a minimal planning setup in which the mechanisms learned by an architecture can be isolated and studied under control.

In this setting, [Bachmann et al. \(2024\)](#) revealed that AR LLMs, based on Transformers ([Vaswani et al., 2017](#)) and State-Space Models ([Gu & Dao, 2024](#); [Dao & Gu, 2024](#)), systematically fail to learn the task, defaulting to random guessing at critical junction vertices. This failure suggests a fundamental limitation in learning complex lookahead tasks. Crucially, they observed that AR models could solve the task when the prediction order was reversed (junction-free), suggesting the difficulty lies in the specific directionality of the planning challenge rather than the graph structure itself.

In this work, we investigate whether Non-Autoregressive (NAR) generative models offer a more suitable paradigm for planning by fundamentally altering the computational nature of the problem. We identify a critical structural asymmetry in the Star-Path planning task: while forward planning involves resolving complex ambiguities at branching junctions, the reverse process, tracing from a known goal back to the start, is often deterministic and junction-free. Unlike AR models, which are constrained to left-to-right generation, NAR models possess the decoding flexibility to exploit this asymmetry, potentially converting difficult long-distance lookahead into first-order neighbor transitions.

In our analysis, we focus on Discrete Diffusion Models (dLLMs), a recently developed class of generative models that has shown promise in various domains ([Campbell et al., 2022](#); [2024](#)). Unlike their autoregressive counterparts, dLLMs are bi-directional and generate complete sequences, iteratively refining the entire sequence from noise. Although this training paradigm requires models to solve a more complex task ([Kim et al., 2025](#)), recent work has shown that this complexity improves the planning ability of such models ([Ye et al., 2024a](#); [Nie et al., 2025](#); [Ye et al., 2025](#)).

Through the comprehensive study of lookahead-based graph algorithms (see [Fig. 1](#) for depiction), we compare the underlying mechanisms acquired by AR and NAR models when learning to plan. As a result, we provide a glimpse into the inner workings of NAR models and dLLMs in particular, guiding future design of systems that solve complex tasks.

Our contributions are as follows:

1. We show that, contrary to previous results, the Star-Path problem can be solved with perfect accuracy by both AR and NAR models when providing a sufficient number of training examples and enabling gradient

steps on the graph description during training.

2. We find that NAR models naturally acquire the simpler "reverse-decoding" strategy. This highlights how NAR models can exploit their decoding flexibility to implicitly adopt simpler solution mechanisms.
3. By modifying the Star-Path task, we further show that our AR and NAR models learn a fundamentally different solution mechanism for the Star-Path task. While AR models must learn high-order lookahead patterns, first-order relations suffice for NAR models. We further show that this mechanistic simplification alleviates strong constraints set on the training complexity and model size.
4. We finally compare the latent representation resulting from the AR and NAR models and identify major differences, further supporting our claims.

## 2. Related Work

### 2.1. Star-Path: A Textual Graph Algorithm Problem

The Star-Path task represents a key subset of a broader research studying LLMs using textually represented graphs ([Jin et al., 2024](#); [Ye et al., 2024b](#); [Wang et al., 2023](#); [Fatemi et al., 2023](#)), specifically, it aims at isolating planning and reasoning mechanisms through synthetic data ([Bachmann et al., 2024](#); [Saparov et al., 2025](#); [Sanford et al., 2024](#); [Noroozadeh et al., 2025b](#); [Zhang et al., 2022](#)). Within this framework, ([Bachmann et al., 2024](#)) utilized the Star-Path task to argue that standard architectures repeatedly fail at planning, establishing a simplified analogy for studying these limitations.

Building on this, subsequent work has dissected the inner workings of transformer planning; [Frydenlund \(2024\)](#) proved the task is theoretically solvable and demonstrated that encoder-only transformers succeed, implicating the autoregressive constraint as the primary bottleneck. Further studies have investigated the learnability of search versus retrieval ([Saparov et al., 2025](#)), the implicit encoding of geometrical relationships ([Noroozadeh et al., 2025a](#)), and the computational complexity hierarchy of graph reasoning ([Sanford et al., 2024](#)).

### 2.2. Non-Autoregressive Language Models

Although the field has largely converged on autoregressive (AR) models due to their simplicity and scaling, non-autoregressive (NAR) paradigms have re-emerged as a compelling alternative ([Devlin et al., 2019](#); [Raffel et al., 2020](#); [Radford et al., 2018](#); [2019](#); [Brown et al., 2020](#)), most notably through Discrete Diffusion Language Models (dLLMs) ([Campbell et al., 2022](#); [2024](#)). Unlike earlier NAR models, dLLMs combine bidirectional context with generative

capabilities, and recent scaling efforts report performance competitive with state-of-the-art AR baselines at comparable costs (Gat et al., 2024; Nie et al., 2025; Ye et al., 2025).

dLLMs utilize a distinct training–inference paradigm where the model learns to denoise partially corrupted sequences in parallel, learning a broad family of conditional distributions rather than a single left-to-right factorization. This enables generation via iterative denoising, a process that progressively reconstructs the sequence from noise (Gat et al., 2025; Kim et al., 2025; Ben-Hamu et al., 2025). This iterative refinement perspective reimagines generation as a non-sequential process, potentially better suited for planning and reasoning tasks (Ye et al., 2024a).

### 3. Star-Path Sequences

Similarly to (Bachmann et al., 2024), we define each Star-Path example as a triplet of a *graph description*, a pair of *source-target vertices*, and the *unique connecting path*.

As depicted in Fig. 1, a Star-Graph  $G(d, l) := (V_G, E_G)$  is a graph whose vertices ( $V_G$ ) and edges ( $E_G$ ) form a star shape where  $d \in \mathbb{N}$  arms extend from a single center vertex  $v_c \in \mathbb{V}$ , such that each arm has length  $l$ .

Consequently, the set of vertices is defined to be:

$$V_G := \{v_c, v_{1,1}, \dots, v_{1,l-1}, \dots, v_{d-1,l-1}\} \subseteq \mathbb{V} \quad (1)$$

so that  $|V_G| = 1 + d(l - 1)$ . Defining  $\mathbb{V}$  as the global pool of allocatable vertices such that  $|\mathbb{V}| = N$ . The vertices are then connected into a star shape by the set of edges:

$$E_G := \left\{ (v_{i,j-1}, v_{i,j}) \left| \begin{array}{l} i \in [0, d), j \in [1, l), \\ v_{i,0} := v_c, v_{i,j} \in V_G \end{array} \right. \right\} \quad (2)$$

The source-target pair is defined as  $\mathcal{T} := (v_c, v_{t,l-1})$ , where  $v_{t,l-1}$  is a leaf vertex terminating the  $t$ -th arm  $t \in [0, d)$ .

Finally, the connecting path is the ordered (inclusive) sequence of vertices from the source to the target:

$$\mathcal{P} := \{v_{t,i} : i \in [1, l); v_{t,0} := v_c\} \quad (3)$$

Because the source vertex  $v_c$  is connected to  $d$  identical arms, the correct initial transition to  $v_{t,1}$  is highly ambiguous. To generate this single token, an autoregressive model must identify the target vertex  $v_{t,l-1}$  within the context, recognize which arm  $t$  it belongs to, and successfully trace the  $l - 1$  edges back to the center. Thus, a seemingly simple next-token prediction inherently requires an  $\ell^{th}$ -order lookahead operation.

For fixed star parameters  $(d, l)$ , the  $i$ -th datapoint is defined textually as the triplet  $S := [E_{G_i} \parallel \mathcal{T}_i \parallel \mathcal{P}_i]$ , where  $G_i(d, l)$  is constructed by uniformly sampling vertices without repetition from  $\mathbb{V}$ . By fully randomizing vertex allocation,

we prevent the model from exploiting spurious correlations tied to specific identifiers and encourage true role-invariant generalization.

To model datapoints as sequential language, we represent  $\mathbb{V}$  as a set of unique vertex identifiers, each mapped to a distinct token in the vocabulary. We then serialize each instance into a single sequence by listing (1) the edges as consecutive pairs of vertex tokens, (2) the source and target vertices, and (3) the vertices along the path from source to target. Overall, this yields sequences of length,

$$|S| = (2 \cdot |E_{G_i}|) + 2 + (d(l - 1) + 1) \quad (4)$$

Diverging from (Bachmann et al., 2024), and to minimize confounding factors, we do not introduce separator tokens to mark sequence attributes (e.g., boundaries between the edge list, the source–target pair, and the path).

### 4. Experimental Setup

In this work, we train a generative model,

$$LM_\theta(\mathbf{x}_{\text{prefix}}) = P(\mathbf{x}_{\text{path}} | \mathbf{x}_{\text{prefix}}) \quad (5)$$

to generate the correct path given a *prefix* sequence consisting of the graph description and the source–target vertices.

We study both autoregressive and non-autoregressive transformer models, denoted  $LM_{\text{AR},\theta}$  and  $LM_{\text{NAR},\theta}$ , respectively. For the NAR setting, we adopt discrete diffusion models as the modeling paradigm. To make the comparison as controlled as possible, we use a shared transformer backbone based on the DDIT implementation of (Gat et al., 2024; Lipman et al., 2024; Ben-Hamu et al., 2025). To enable AR modeling, we modify the same implementation to (1) use causal self-attention, (2) set the diffusion time embedding to a constant value  $t = 0$ , and (3) replace the diffusion training and sampling procedures with standard AR next-token training and decoding.

Across experiments, we used the same model parameters as GPT-2 (Radford et al., 2019), with  $d_{\text{model}} = 384$ . The vocabulary is defined to be the enumeration of  $\mathbb{V}$ , alongside a [MASK] token. All sequences within each training setup are of a fixed length and are defined by 4. Refer to appendix §A for model specifications.

We experiment with fixed graph parameters (e.g.,  $d, l$ ). For every such parameter setting, we construct a single held-out test set that is shared across all runs. Training examples are generated on-the-fly: we sample unique instances during training, ensuring no repetition and no overlap with the test set. For each run, we record the number of training examples required to reach convergence, and enforce a maximum training budget after which training is terminated. Because

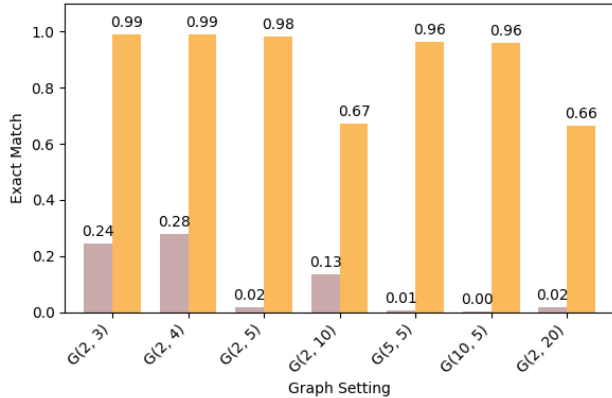


Figure 2. Comparison of AR models trained with (orange) and without (pink) gradients on the graph prefix across graph settings. All models were trained on up-to 50M distinct training examples.

training samples are generated online, no two runs observe the same samples or sample order, which further reduces potential confounding effects.

#### 4.1. Training paradigms

We consider two training regimes:

1. **Conditional training.** The model is conditioned on the prefix (graph description + source–target vertices) and trained only on the path tokens. Concretely, we mask out loss terms on prefix positions so gradients are computed only for the path.
2. **Full-sequence training.** The model is trained to generate the entire sequence (prefix and path). Under this, gradients are computed over all tokens, and therefore, the model is additionally rewarded for learning to generate legal graph descriptions.

At test time, we provide the ground-truth prefix and decode only the path tokens.

#### 4.2. Success Criteria

We measure convergence using an *exact-match* metric. A prediction is counted as correct only if the entire predicted path matches the ground-truth path token-by-token. Let  $\tilde{\mathbf{x}}_{\text{path}} = LM_{\theta}(\mathbf{x}_{\text{prefix}})$ . Then, for a test set  $\mathbb{D}$ ,

$$S := \frac{\sum_{(\mathbf{x}_{\text{prefix}}, \mathbf{x}_{\text{path}}) \in \mathbb{D}} \mathbf{1}\{\tilde{\mathbf{x}}^i = \mathbf{x}_{\text{path}}^i : i \in [0, l]\}}{|\mathbb{D}|} \quad (6)$$

where  $\mathbf{x}^i$  denotes the  $i$ -th token in the sequence  $\mathbf{x}$ .

## 5. Findings

In this section, we present our empirical results analyzing the distinct planning mechanisms acquired by Autoregressive (AR) and Non-Autoregressive (NAR) models, comparing their convergence behaviors, underlying solution strategies, and internal latent representations on the lookahead task.

### 5.1. Learnability of The Star-Path

Contrary to recent claims suggesting that AR models are fundamentally incapable of solving lookahead planning tasks (Bachmann et al., 2024), our results demonstrate that standard AR Transformers can learn the Star-Path task with perfect accuracy. We posit that the previously reported failures are not due to inherent structural limitations of the architecture, but rather stem from the optimization signal provided during training. Specifically, we identify that the learnability of the task heavily depends on whether the model is incentivized to internalize the graph structure.

To isolate this effect, we compare two training objectives. The standard approach models the conditional probability  $p(\text{path}|\text{prefix})$ , where the prefix (graph description and source-target pair) is provided as a prompt context without gradient propagation on its tokens. While theoretically sufficient, we find that this formulation renders the optimization landscape difficult to traverse, leading to slow or stalled convergence. In contrast, as can be seen in Fig. 2, by enabling gradient propagation on the prefix and treating the graph description as part of the generative modeling task, we observe a dramatic acceleration in convergence. Although the precise dynamics of this, pre-training-like, phenomenon warrant further investigation, it suggests that forcing the model to explicitly model the graph structure rather than merely attending to it is crucial for acquiring the necessary lookahead mechanisms.

However, we observe that even with this optimized objective, fully mastering the task necessitates a substantial volume of training data. In our experiments, we capped the training budget at 50M sequences, an order of magnitude more than previous work (capped at 200K with multiple epochs). This indicates that while learnable, the task remains sample-inefficient for AR architectures. Furthermore, we observe that for graph configurations, even this extensive budget occasionally proved insufficient. Crucially, all models are trained for a single epoch over non-repeating data streams. This strict regime ensures the model cannot overfit to specific training instances, further establishing that our reported results reflect generalization rather than memorization.

Fig. 2 illustrates the empirical impact of this training choice across varying graph complexities. We compare the Exact Match accuracy of AR models trained with and without

prefix gradients on an equal number of examples (50M). The results reveal a stark disparity: models trained with prefix gradients (orange bars) were able to achieve near-perfect accuracy ( $> 0.95$ )<sup>1</sup> on most settings. Conversely, the baseline approach (pink bars) fails to converge. These findings demonstrate that the primary bottleneck in AR planning is not the search capacity, but the richness of the supervision signal provided during training.

### 5.2. Mechanistic Adaptability

A central question in our study is how NAR models manage to more efficiently solve lookahead tasks that theoretically require high-order planning. By attributing an associative memory structure to transformers (Bietti et al., 2023; Radhakrishnan et al., 2020), we hypothesize that the underlying mechanism used to solve the task involves learning a lookup table that is then traversed at inference time. Consequently, resolving which branching arm leads from the source to the target leaf fundamentally requires the model to evaluate  $\ell^{th}$ -order lookahead relations ( $\ell$  being the arm length). We thus conjecture that AR models, which are restricted to the causal order of the path, are forced to represent a complex data structure of magnitude  $O(\ell)$ .

While the forward path from the center vertex  $v_c$  to the target leaf  $v_{t,l-1}$  is highly ambiguous and requires lookahead, the reverse path from the target leaf back to the center is deterministic and junction-free. Hence, we further hypothesize that NAR models may be able to leverage their flexible decoding trajectory and adapt a strategy that exploits the structural asymmetry of the lookahead task. As a result, learn a simpler  $O(1)$  data structure.

To show this, in the following, we analyze the training and inference dynamics of AR and NAR models trained on the lookahead task. Fig. 3 visualizes the decoding process of our NAR model (dLLM; see §4). The x-axis represents the vertex position in the path, and the y-axis represents the decoding step. Color indicates the percentage of examples where a specific token was unmasked (predicted) at a given step. Across multiple graph settings, we observe a striking and consistent diagonal pattern moving from the bottom-right to the top-left. This indicates that the NAR model naturally adopts an anti-causal decoding strategy, a mechanism impossible for a standard AR model, prioritizing the unmasking of the target-end tokens first. Thus, the NAR model can indeed suffice with  $1^{st}$ -order neighbor transitions, supporting our hypothesis.

Fig. 4 compares the training dynamics between AR and NAR models, depicting the convergence of vertex predic-

<sup>1</sup>To reduce computational and environmental costs, runs maintaining a convergence score higher than 0.95 for 10 consecutive evaluation steps were terminated early.

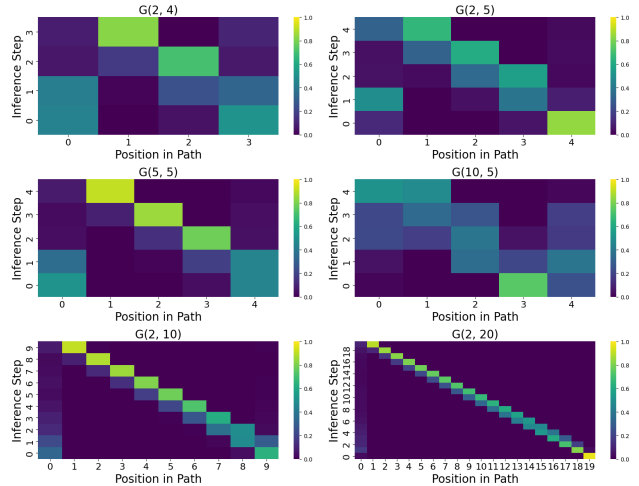


Figure 3. A visualization of the dLLM’s NAR decoding process across different graph settings. The x-axis represents the vertex position in the path, and the y-axis represents the decoding step. Color indicates the percentage of examples where a specific token was unmasked (predicted) at a given step.

tion along the path, on average across the test set. Multiple graph configurations are shown. As can be seen, both AR and NAR models quickly learn to predict the path endpoints correctly (a simple copying mechanism from the task description). However, the way they learn to correctly predict the intermediate vertices differs fundamentally. The AR model exhibits a “bottleneck” behavior, struggling with the intermediate path for a significant portion of training, followed by a simultaneous emergence of all middle vertices. Assuming  $1^{st}$ -order transitions are learned first, an autoregressive model must nevertheless wait for the  $\ell^{th}$ -order task to be solved before the simpler transition operation becomes applicable, causing the observed bottleneck.

In contrast, the NAR model demonstrates incremental learning, steadily predicting vertices starting from the end of the path and moving backwards. This further facilitates the adaptability of the decoding trajectory to the simpler solution formulation. Moreover, by solving easier sub-tasks earlier and utilizing those solutions as context for preceding vertices, the model implements an alternative learning pattern de facto.

These results highlight one inherent difference in the way AR and NAR models operate. This flexibility enables NAR models to solve tasks in a fundamentally different manner, often accelerating learning by adopting a simpler and more efficient solution mechanism.

### 5.3. A Simpler Underlying Mechanism

Building on the hypothesis introduced in Section 5.2, we further investigate the emergence of  $1^{st}$ -order and  $\ell^{th}$ -order mechanisms within these models. We achieve this by ma-

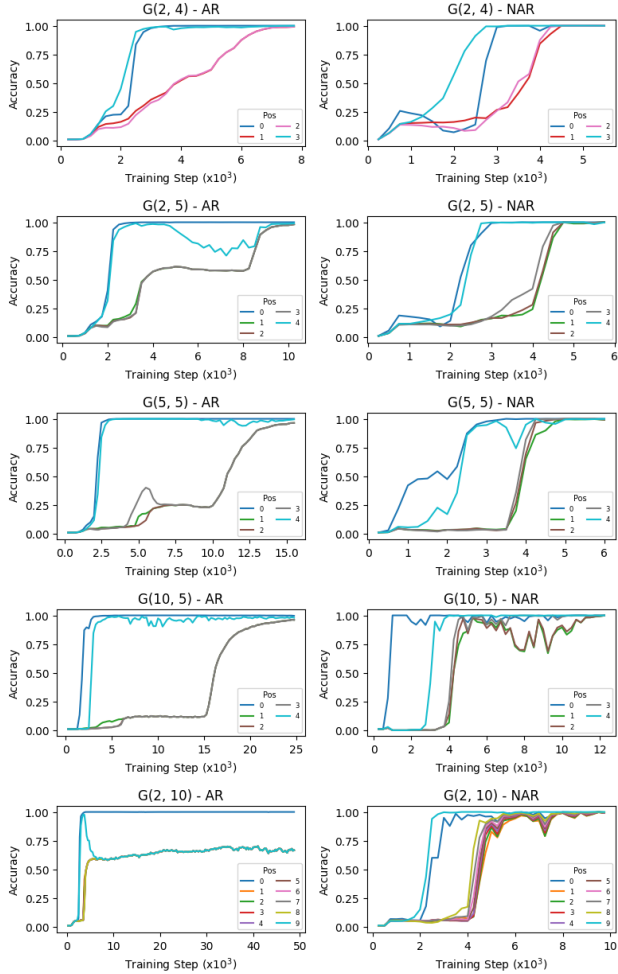


Figure 4. A comparison of the training dynamics of AR and NAR models depicting the per-position (vertex) average accuracy over the test set. Note that “ $G(2,10) - AR$ ” did not reach convergence. For visualization purposes, the x-axis scale varies across.

nipulating the lookahead task definition to isolate specific solution strategies and tracking the required number of training samples for convergence.

We first analyze exact-match accuracy during training for the standard Star-Path configuration, where the model generates a path from the center vertex to a leaf. Figure 5 illustrates results across four graph settings, revealing two key insights. First, NAR models demonstrate superior sample efficiency, converging significantly faster than their AR counterparts, a trend consistent across all experimental runs. Second, while NAR models exhibit a single, rapid transition from zero to perfect accuracy, AR models undergo two distinct “jumps” before convergence. Notably, the first AR jump coincides temporally with NAR convergence. This intermediate plateau in AR performance aligns with the findings of (Bachmann et al., 2024), characterizing a strategy where the model randomly selects an initial vertex and correctly

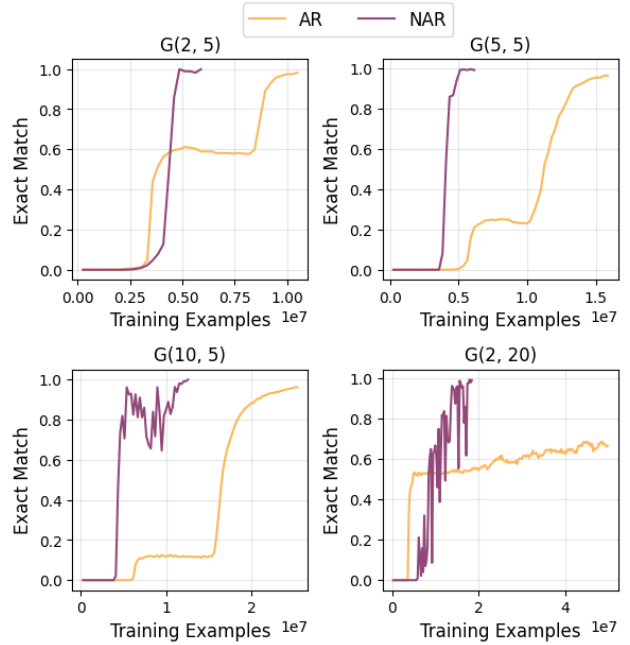


Figure 5. Training convergence comparison between AR and NAR models across varying graph complexities ( $G(d, l)$ ). The y-axis denotes the exact-match accuracy on a held-out test set, while the x-axis indicates the number of unique training examples observed.

traverses the subsequent deterministic path (resulting in  $1/d$  accuracy). Taken together with the “bottleneck” effect discussed in Section 5.2, these dynamics strongly suggest that the two paradigms utilize fundamentally different lookahead mechanisms.

Figure 6a (upper-left) quantifies this disparity by plotting the number of training samples required for convergence against the number of associative connections in the graph. Under an associative memory framework, learning both  $1^{st}$ -order and  $\ell^{th}$ -order lookahead necessitates internalizing all possible mappings, leading to an exponential scaling with graph complexity. Our results show a widening gap in sample efficiency between AR and NAR models as the number of associative connections increases.

To further delineate these mechanisms, we introduced two task variants designed to isolate  $1^{st}$ -order and  $\ell^{th}$ -order strategies. Both variants maintain the original prefix structure (graph description and source-target pair) but modify the required output:

**$1^{st}$ -Order Task:** In this variant, models generate the path from the leaf vertex back to the center vertex (Figure 6b, upper-right). Because the reverse direction is deterministic and junction-free, both AR and NAR models can succeed using only  $1^{st}$ -order transitions. As expected, both models exhibit nearly identical convergence curves, confirming that both are capable of learning local transitions with equal

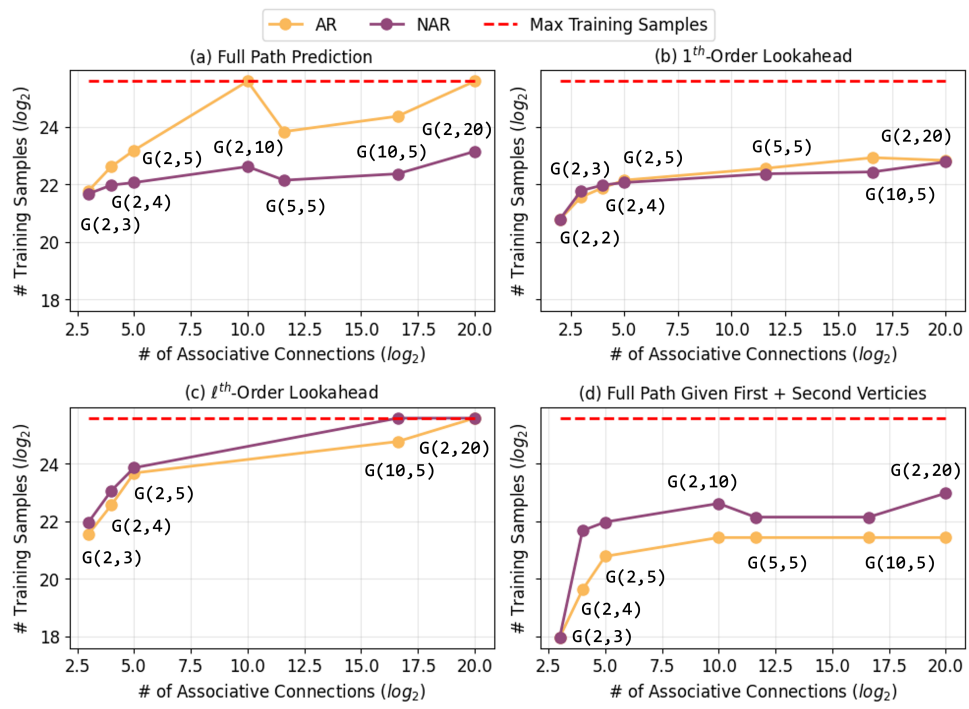


Figure 6. Analysis of 1st-order vs.  $\ell^{\text{th}}$ -order lookahead mechanisms across varying graph sizes. The x-axis represents the number of associative connections ( $\log_2$ -scale), and the y-axis shows the number of training samples ( $\log_2$  scale) required for convergence. (a) Models are trained on the original task ; (b) Models are trained on the 1<sup>st</sup>-Order Lookahead task ; (c) Models are trained on the  $\ell^{\text{th}}$ -Order Lookahead task ; (d) Models are trained on the “Hinted” task. Graph settings are noted next to their datapoint. The red line indicates the maximum training examples (50M); a model reaching this point is terminated, and its convergence is inconclusive.

efficiency when long-range lookahead is not required.

**$\ell^{\text{th}}$ -Order Task:** Conversely, we require the models to predict only the second vertex in the forward path, the critical junction choice, given only the prefix. This removes the possibility of NAR reverse-decoding, forcing both models to resolve the long-range dependency immediately. Figure 6c (lower-left) shows that in this  $\ell^{\text{th}}$ -order setting, NAR models lose their sample efficiency advantage and converge at rates similar to AR models, reinforcing the hypothesis that NAR’s typical advantage stems from bypassing  $\ell^{\text{th}}$ -order dependencies.

**“Hinted Task”:** Finally, we evaluate the original forward task using a “hinted” decoding procedure (Figure 6d, lower-right). Here, the models are trained normally but are provided with the first two vertices of the path as context during inference. This setup allows a model that has only mastered 1<sup>st</sup>-order transitions to achieve perfect accuracy. Both paradigms reach convergence on this task within a similar timeframe, corresponding to the initial learning phase of the NAR model and the first jump in AR performance.

These findings demonstrate that AR and NAR models leverage fundamentally different strategies for planning. While the causal constraints of AR models necessitate the mastery of  $\ell^{\text{th}}$ -order transitions, NAR models exploit their decoding

flexibility to solve the task via simpler 1<sup>st</sup>-order mechanisms. This simplification not only accelerates convergence but also, as suggested by (Sanford et al., 2024), reduces the computational complexity of the problem, potentially alleviating the need for the extreme model depth and width typically required for complex graph traversal.

#### 5.4. Latent Space Implications

To further investigate the internal representations that facilitate these distinct planning mechanisms, we analyzed the latent encodings generated by the models during inference. Specifically, we sought to understand how the models represent the graph topology and vertex identities within their embedding space.

We extracted the hidden states for each vertex token across the network’s layers. Since a vertex appears multiple times within a graph description, we computed a single aggregate embedding for each vertex by averaging the representations of all its token occurrences in the input sequence. We then applied Principal Component Analysis (PCA) to project these high-dimensional embeddings into a 2D space for visualization.

We visualize these projections using two distinct coloring

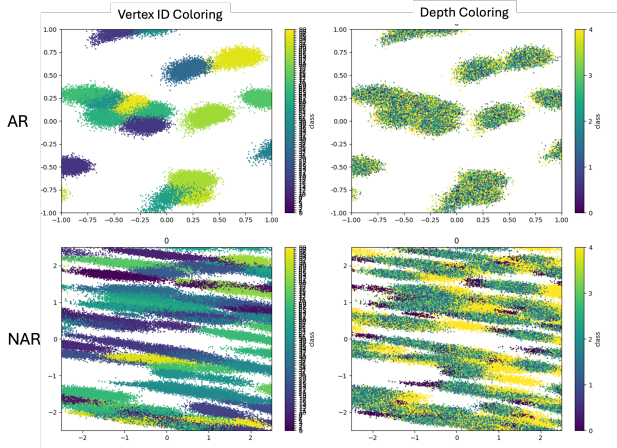


Figure 7. Zoomed-in analysis of Layer 0 embeddings. While both models cluster by vertex ID (Left), the NAR model (Bottom-Right) organizes these clusters into clear gradients based on topological depth. The AR model (Top-Right) shows no such internal structure, highlighting the NAR advantage of bidirectional context.

schemes. **Depth Coloring:** Vertices are colored based on their topological distance from the center vertices  $v_c$ . (Purple indicates the center vertex, while Yellow indicates leaf vertices). **Vertex ID Coloring:** Vertices are colored based on their unique identifier token in the vocabulary. All visualizations were generated using the  $G(5, 5)$  graph setting.

Figure 8 presents the evolution of the latent space across layers with points colored by topological depth. We observe that the AR model (top row) rapidly disentangles the graph structure in the early layers, creating distinct clusters for center vertices (purple) and leaf vertices (yellow). This separation is maintained and refined through the deeper layers, suggesting that the AR model explicitly constructs and preserves a “depth-map” of the graph to facilitate its sequential lookahead.

In contrast, the NAR model (bottom row) exhibits a strikingly different pattern. While it also separates distinct depths in the initial layers (Layers 0-3), this clear structural distinction appears to dissolve in the deeper layers (Layers 4-11). The representation becomes more diffuse, with no clear separation between center, leaf, and intermediate vertices. This behavior aligns with our previous findings, as the NAR model relies on a simpler  $1^{st}$ -order neighbor traversal (reverse decoding), it may not require a deep, persistent representation of the global hierarchy, unlike the AR model, which must maintain long-range dependencies to solve the  $l^{th}$ -order forward task.

Figure 9 in Appendix B visualizes the same embeddings colored by vertex ID. Since vertex identifiers are assigned randomly to graph positions, a robust planner should ideally abstract away from specific IDs. However, we observe that both models initially cluster vertices heavily by their

identity.

The AR model (top row) shows strong ID-based clustering in Layer 0, but this organization degrades quickly as the model progresses, presumably as it overwrites identity information with the learned topological relationships required for planning. Conversely, the NAR model (bottom row) preserves this identity-based clustering for significantly longer, maintaining clear separation through the middle layers. This suggests that the NAR model’s solving mechanism is more “local,” relying on specific token identities to perform immediate neighbor matching rather than abstracting them into a global structural schema. Figure 7 in Appendix B provides a high-resolution view of the first layer (Layer 0) comparisons, revealing an important mechanism enabled by non-autoregressive processing.

Both models exhibit the expected clustering by Node ID (Left column), a natural consequence of the embedding initialization. However, the internal structure of these clusters differs fundamentally. In the AR model (top-right), the distribution of topological depths within a Node ID cluster is unstructured and noisy.

In contrast, the NAR model (bottom-right) displays a clear, organized gradient within each Node ID cluster, where vertices are arranged linearly by their depth (transitioning from yellow to purple). This structured “stripe” pattern indicates that the NAR model successfully encodes the vertex’s role (depth) alongside its identity immediately in the first layer.

This phenomenon is a direct result of the NAR model’s bidirectional attention mechanism. Unlike the AR model, which is causally masked and must infer structure sequentially, the NAR model has access to the full graph description simultaneously. This allows it to contextualize a vertex with its global position in the graph immediately, “pre-computing” the topological relationships before the deep processing even begins. This early access to structural context likely facilitates the simpler solution path observed in our convergence experiments.

## 6. Discussion

We investigated the internal mechanisms of autoregressive (AR) and Discrete Diffusion based non-autoregressive (NAR) models on lookahead planning tasks. Contrary to claims that AR models are structurally incapable of such planning, we demonstrate that both paradigms can achieve perfect accuracy when provided with sufficient data and a structure-enforcing objective. However, they arrive at the solution through fundamentally different paths.

Our analysis reveals that AR models, constrained by causal directionality, hit a “learning bottleneck” as they are forced to master complex  $l^{th}$ -order lookahead patterns. In contrast,

NAR models demonstrate remarkable flexibility by exploiting structural asymmetry: they naturally adopt a "reverse-decoding" strategy that reduces the high-order challenge to simple 1<sup>st</sup>-order neighbor transitions. This allows NAR models to converge with exponentially fewer training examples.

Ultimately, our findings highlight the unique potential of NAR models, particularly the emerging class of Discrete Diffusion Models, to bypass the sequential constraints that hinder standard transformers in planning scenarios. Yet, an open question remains: while NAR models exhibit superior performance and efficiency, it is unclear if they possess an inherently superior capacity for planning. Our results provide a compelling example where flexibility enables a more efficient solution (via 1<sup>st</sup>-order lookahead) rather than necessarily solving the general  $\ell^{\text{th}}$ -order problem, where AR and NAR models might behave similarly. Given that AR models are theoretically capable of solving the task given enough capacity and supervision, future work must further disentangle whether the NAR advantage is one of fundamental reasoning capability or strictly one of exploiting varying computational paths to the same solution.

## Impact statement

This paper advances the understanding of autoregressive and non-autoregressive architectures for language modeling, contributing to the broader field of Machine Learning. There are many potential societal consequences of our work, none of which we feel must be specifically highlighted here.

## References

- Bachmann, G. et al. The pitfalls of next-token prediction. In *International Conference on Machine Learning*, pp. 2296–2318. PMLR, 2024.
- Ben-Hamu, H., Gat, I., Severo, D., Nolte, N., and Karrer, B. Accelerated sampling from masked diffusion models via entropy bounded unmasking. *arXiv preprint arXiv:2505.24857*, 2025.
- Bietti, A., Cabannes, V., Bouchacourt, D., Jegou, H., and Bottou, L. Birth of a transformer: A memory viewpoint. *Advances in Neural Information Processing Systems*, 36: 1560–1588, 2023.
- Brown, T. B., Mann, B., Ryder, N., Subbiah, M., Kaplan, J., Dhariwal, P., Neelakantan, A., Shyam, P., Sastry, G., Askell, A., Agarwal, S., Herbert-Voss, A., Krueger, G., Henighan, T., Child, R., Ramesh, A., Ziegler, D., Wu, J., Winter, C., Hesse, C., Chen, M., Sigler, E., Litwin, M., Gray, S., Chess, B., Clark, J., Berner, C., McCandlish, S., Radford, A., Sutskever, I., and Amodei, D. Language models are few-shot learners. *Advances in Neural Information Processing Systems*, 33, 2020. URL <https://arxiv.org/abs/2005.14165>.
- Campbell, A., Benton, J., De Bortoli, V., Rainforth, T., Deligiannidis, G., and Doucet, A. A continuous time framework for discrete denoising models. *Advances in Neural Information Processing Systems*, 35:28266–28279, 2022.
- Campbell, A., Yim, J., Barzilay, R., Rainforth, T., and Jaakkola, T. Generative flows on discrete state-spaces: Enabling multimodal flows with applications to protein co-design. *arXiv preprint arXiv:2402.04997*, 2024.
- Dao, T. and Gu, A. Transformers are ssms: Generalized models and efficient algorithms through structured state space duality. *arXiv preprint arXiv:2405.21060*, 2024.
- Devlin, J., Chang, M.-W., Lee, K., and Toutanova, K. Bert: Pre-training of deep bidirectional transformers for language understanding. In *Proceedings of the 2019 Conference of the North American Chapter of the Association for Computational Linguistics: Human Language Technologies*, 2019. URL <https://arxiv.org/abs/1810.04805>.
- Erdogan, L. E., Furuta, H., Kim, S., Lee, N., Moon, S., Anumanchipalli, G., Keutzer, K., and Gholami, A. Plan-and-act: Improving planning of agents for long-horizon tasks. In *Forty-second International Conference on Machine Learning*, 2025.
- Fatemi, B., Halcrow, J., and Perozzi, B. Talk like a graph: Encoding graphs for large language models, 2023.
- Frydenlund, A. The mystery of the pathological path-star task for language models, 2024.
- Gao, C., Lan, X., Li, N., Yuan, Y., Ding, J., Zhou, Z., Xu, F., and Li, Y. Large language models empowered agent-based modeling and simulation: A survey and perspectives. *Humanities and Social Sciences Communications*, 11(1):1–24, 2024.
- Gat, I., Remez, T., Shaul, N., Kreuk, F., Chen, R. T., Synnaeve, G., Adi, Y., and Lipman, Y. Discrete flow matching. *Advances in Neural Information Processing Systems*, 37:133345–133385, 2024.
- Gat, I., Ben-Hamu, H., Havasi, M., Haziza, D., Reizenstein, J., Synnaeve, G., Lopez-Paz, D., Karrer, B., and Lipman, Y. Set block decoding is a language model inference accelerator. *arXiv preprint arXiv:2509.04185*, 2025.
- Gu, A. and Dao, T. Mamba: Linear-time sequence modeling with selective state spaces. In *First conference on language modeling*, 2024.

- Jin, B. et al. Large language models on graphs: A comprehensive survey. *IEEE Transactions on Knowledge and Data Engineering*, 2024.
- Kim, J., Shah, K., Kontonis, V., Kakade, S., and Chen, S. Train for the worst, plan for the best: Understanding token ordering in masked diffusions. *arXiv preprint arXiv:2502.06768*, 2025.
- Lipman, Y., Havasi, M., Holderrieth, P., Shaul, N., Le, M., Karrer, B., Chen, R. T., Lopez-Paz, D., Ben-Hamu, H., and Gat, I. Flow matching guide and code. *arXiv preprint arXiv:2412.06264*, 2024.
- Nie, S., Zhu, F., You, Z., Zhang, X., Ou, J., Hu, J., Zhou, J., Lin, Y., Wen, J.-R., and Li, C. Large language diffusion models. *arXiv preprint arXiv:2502.09992*, 2025.
- Noroozizadeh, S., Nagarajan, V., Rosenfeld, E., and Kumar, S. Deep sequence models tend to memorize geometrically; it is unclear why. *arXiv preprint arXiv:2510.26745*, 2025a.
- Noroozizadeh, S. et al. Deep sequence models tend to memorize geometrically; it is unclear why, 2025b.
- Radford, A., Narasimhan, K., Salimans, T., and Sutskever, I. Improving language understanding by generative pre-training. OpenAI technical report, 2018. URL [https://cdn.openai.com/research-covers/language-unsupervised/language\\_understanding\\_paper.pdf](https://cdn.openai.com/research-covers/language-unsupervised/language_understanding_paper.pdf).
- Radford, A., Wu, J., Child, R., Luan, D., Amodei, D., Sutskever, I., et al. Language models are unsupervised multitask learners. *OpenAI blog*, 1(8):9, 2019.
- Radhakrishnan, A., Belkin, M., and Uhler, C. Overparameterized neural networks implement associative memory. *Proceedings of the National Academy of Sciences*, 117(44):27162–27170, 2020.
- Raffel, C., Shazeer, N., Roberts, A., Lee, K., Narang, S., Matena, M., Zhou, Y., Li, W., and Liu, P. J. Exploring the limits of transfer learning with a unified text-to-text transformer. *Journal of machine learning research*, 21(140):1–67, 2020.
- Sanford, C., Fatemi, B., Hall, E., Tsitsulin, A., Kazemi, M., Halcrow, J., Perozzi, B., and Mirrokni, V. Understanding transformer reasoning capabilities via graph algorithms. *Advances in Neural Information Processing Systems*, 37:78320–78370, 2024.
- Saparov, A., Pawar, S. A., Pimpalgaonkar, S., Joshi, N., Pang, R. Y., Padmakumar, V., Kazemi, M., Kim, N., and He, H. Transformers struggle to learn to search. In *The Thirteenth International Conference on Learning Representations*, 2025.
- Valmeekam, K., Marquez, M., Sreedharan, S., and Kambhampati, S. On the planning abilities of large language models—a critical investigation. *Advances in Neural Information Processing Systems*, 36:75993–76005, 2023.
- Vaswani, A., Shazeer, N., Parmar, N., Uszkoreit, J., Jones, L., Gomez, A. N., Kaiser, Ł., and Polosukhin, I. Attention is all you need. *Advances in neural information processing systems*, 30, 2017.
- Wang, H. et al. Can language models solve graph problems in natural language? In *Advances in Neural Information Processing Systems*, volume 36, pp. 30840–30861, 2023.
- Ye, J., Gao, J., Gong, S., Zheng, L., Jiang, X., Li, Z., and Kong, L. Beyond autoregression: Discrete diffusion for complex reasoning and planning. *arXiv preprint arXiv:2410.14157*, 2024a.
- Ye, J., Xie, Z., Zheng, L., Gao, J., Wu, Z., Jiang, X., Li, Z., and Kong, L. Dream 7b: Diffusion large language models. *arXiv preprint arXiv:2508.15487*, 2025.
- Ye, R. et al. Language is all a graph needs. In *Findings of the Association for Computational Linguistics: EACL 2024*, 2024b.
- Zhang, Y. et al. Unveiling transformers with lego: A synthetic reasoning task, 2022.

## A. AR and NAR Implementation Specifications

Our implementation of an autoregressive and non-autoregressive model was based on the Flow-Matching repo<sup>2</sup>. To enable comparable AR and NAR modeling, we have modified the training and inference implementations to standard autoregressive procedures based on the same architecture. The following are the model parameters used for training the AR and NAR models:

Table 1. Configuration hyperparameters.

Parameter	AR	NAR
Causal Masking	✓	×
Autoregressive Decoding	✓	×
Batch Size	1024	
Max. Training Examples	$50 \times 10^6$	
Optimizer	AdamW	
Learning Rate	$3 \times 10^{-4}$	
$\beta_1$	0.9	
$\beta_2$	0.95	
$\epsilon$	$1 \times 10^{-8}$	
Weight Decay	0.03	
Warmup Steps	$5 \times 10^3$	
Grad Clip	1.0	
$\eta_{\min}$ Ratio	0.01	
Accumulation Steps	1	
Loss Function	Cross Entropy	
Source Distribution	Masked Seq.	×
Scheduler Type	Polynomial	×
Hidden Size	384	
Cond. Dim.	4	
# Transformer Blocks	12	
# Attention Heads	6	
Dropout	0.1	

<sup>2</sup>[https://github.com/facebookresearch/flow\\_matching](https://github.com/facebookresearch/flow_matching)

## B. Latent Space Implications - Additional Results

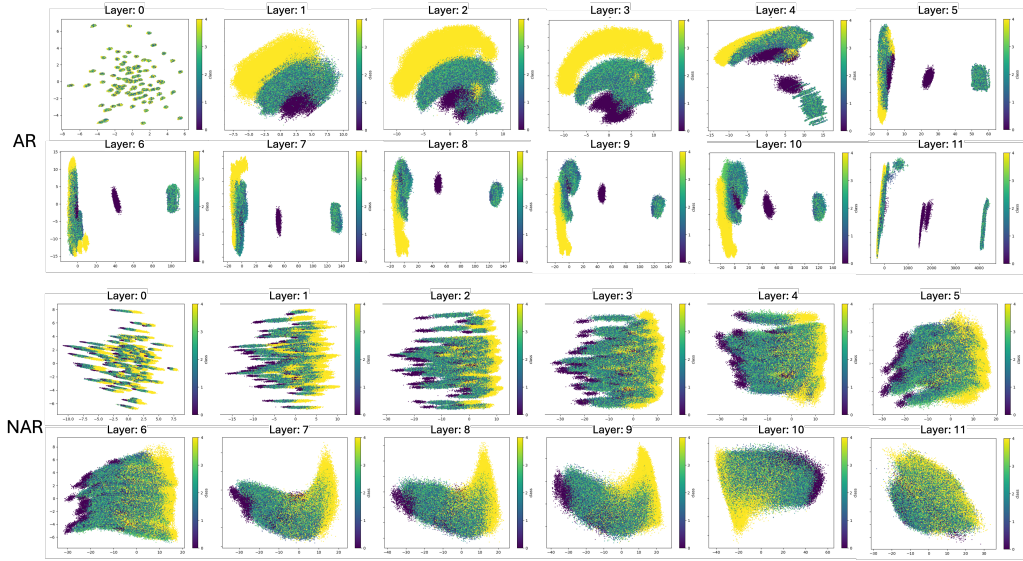


Figure 8. PCA projection of latent representations across layers for AR (top) and NAR (bottom) models on  $G(5, 5)$ . Points are colored by topological depth (Purple: Center, Yellow: Leaf). While AR maintains structural separation deep into the network, NAR’s structural representation becomes diffuse in later layers.

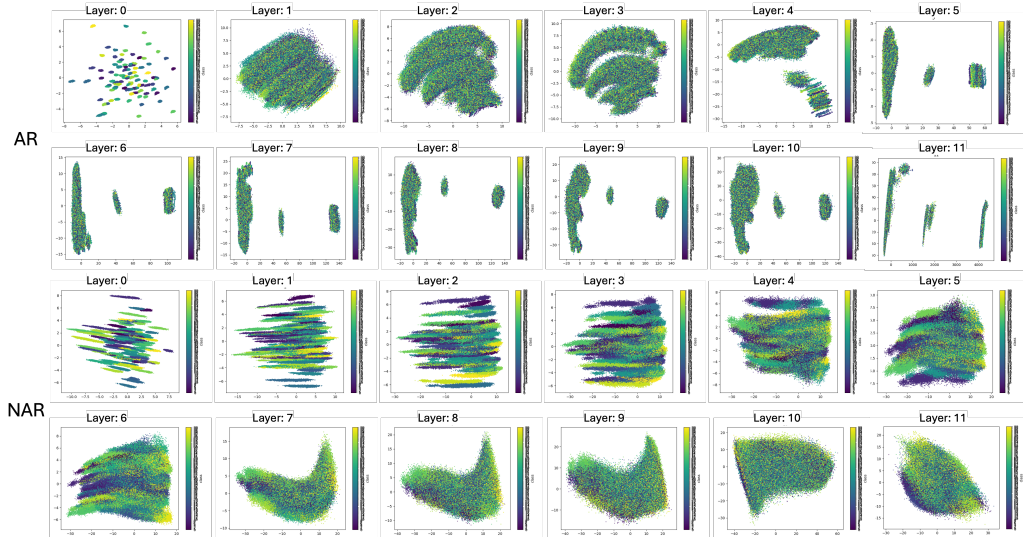


Figure 9. PCA projection of latent representations colored by vertex ID. NAR models (bottom) preserve identity-based clustering deeper into the network compared to AR models (top), suggesting a reliance on local identity matching.